CHAPTER 5 (PAGES 119-159)
STRATIFIED FLOW OVER TOPOGRAPHY

Ronald B. Smith
Yale University, New Haven, Connecticut, USA

1. INTRODUCTION

The analytical study of stratified airflow over hills began with G. Lyra in Germany (1943). Lyra was recruited by L. Prandtl to investigate the pioneering 1933 wave-assisted 7000-meter glider ascent by J. Kuettner. Kuettner published his observations and interpretations of mountain waves and wave clouds in 1939. P. Queney, then at the University of Chicago, joined the effort shortly thereafter (1947). Their fundamental theoretical contributions showed how airflow over mountains could generate steady gravity waves; waves whose restoring force arises from the background gravitational stability of the atmosphere. They established a consistent small-amplitude theory of mountain waves. In 1949, R. Scorer discovered that if the wind speed increased or the stability decreased with height, that a gravity wave "resonant cavity" could be formed between the jet stream aloft and the earth's solid surface. In this situation, trapped periodic "lee waves" would be generated by the hills and extend downstream for a considerable distance. During the period 1940 to 1955, the mathematical and physical issues of energy radiation, causality and the appropriate upper boundary condition for solution uniqueness were hotly debated and finally resolved (Eliassen and Palm, 1954). In the 1950's, R. Long showed that under special circumstances, finite amplitude disturbances could be treated analytically (1953, 1955). All of these remarkable early contributions were summarized in a technical note of the World Meteorological Organization (Queney et al., 1960). Since that time, research on the subject has expanded rapidly, encouraged by practical applications to aviation safety, severe wind damage and atmospheric mixing. Mountain waves have also been studied to understand their contribution to the momentum balance of the atmosphere. Corresponding phenomena in the stratified ocean have also been studied. There is no doubt that the beauty of wave clouds and the intrinsic elegance of the mathematical analyses have also stimulated this work.

In the development of lee wave theory, a great debt is owed to Rayleigh, Kelvin and other mathematical physicists from the previous century who showed that acoustic, electromagnetic and surface gravity waves could be treated analytically. In spite of this solid foundation, the effort to understand lee waves has been challenging, due to the dispersive and anisotropic nature of internal gravity waves. The study of complex linear and nonlinear wave dynamics has been aided by rapid advances in the numerical simulation of wave-like flows (Durran, 1998, Doyle et al., 2000). Extensive reviews of mountain wave dynamics have been given by Smith (1979, 1989a), Durran (1990), and Wurtele et al. (1996). Lee wave theory has also been discussed in textbooks on atmospheric dynamics (Gill, 1982), stratified flow (Turner, 1973), mesoscale meteorology (Atkinson, 1981 and Durran, 1986a) and atmospheric waves (Gossard and Hooke, 1975). The most complete treatment of this field is the monograph by P. Baines (1995). Baines describes layered flow, 2-dimensional flow, upstream blocking and laboratory experiments among other subjects.

In this Chapter, we present the basic theory of mountain waves, with an emphasis on newer developments. We use a new more flexible linear theory model to illustrate the various physical attributes of lee waves. We also discuss recent work on non-linear dissipative lee wave dynamics. Special attention is placed on the subject of potential vorticity generation, an issue that has arisen in the last decade.

2. INTERNAL GRAVITY WAVES AND GROUP VELOCITY

The basic properties of internal gravity waves have been discussed elsewhere (e.g. Turner, 1973, Gossard and Hooke, 1975, Gill, 1982) and in other chapters of this book. Here we give a brief review of the subject as a foundation for mountain wave theory. The linearized Boussinesq equations for waves in a stagnant stably stratified fluid are:

$$u_t = -(1/\rho_0)p_x \qquad \text{x-momentum} \qquad (1a)$$

$$v_t = -(1/\rho_0)p_y \qquad \text{y-momentum} \qquad (1b)$$

$$w_t = -(1/\rho_0)p_z - (g/\rho_0)\rho' \qquad \text{z-momentum} \qquad (1c)$$

$$u_x + v_y + w_z = 0 \qquad \text{continuity} \qquad (1d)$$

$$\rho'_t + (d\rho / dz)w = 0 \qquad\qquad \text{density conservation} \qquad (1e)$$

governing the five fluctuating fields u(x,y,z,t), v(x,y,z,t), w(x,y,z,t), p(x,y,z,t) and ρ'(x,y,z,t). The "z" coordinate is directed upward, opposite to the gravity vector. Subscripts indicate partial derivatives. The Boussinesq formulation neglects density variations in the inertial terms and the kinematic divergence of the velocity field associated with compressibility. Density variations play a role only through the action of gravity. The buoyancy effect is proportional to the value of the buoyancy frequency N defined by

$$N^2 = (-g / \rho_0)(d\rho / dz)$$

The quantity ρ_0 is a reference density. The quantity $(d\rho/dz)$ is the ambient vertical gradient in density. A similar set of equations to (1) can be derived for a compressible atmosphere using scaled variables. In this case, the buoyancy frequency is written

$$N^2 = (g / \theta)(d\theta / dz)$$

where the potential temperature is given by $\theta = T(p_0 / p)^{(\gamma-1)/\gamma}$.

If the coefficients in (1) are constant, it has plane-wave solutions with each dependent variable written in the complex exponential form. For example, the vertical velocity is written

$$w(x, y, z, t) = \text{Re}[\hat{w} \cdot \text{expi}(kx + ly + mz - \omega t)] \qquad (2)$$

In (2), k, l and m are the three components of the wavenumber vector,

$$\vec{\kappa} = k\vec{i} + l\vec{j} + m\vec{k} \qquad (3)$$

whose magnitude is

$$|\vec{\kappa}| = (k^2 + l^2 + m^2)^{1/2} \qquad (4)$$

The plane wave expressions satisfy (1) if the frequency ω(k,l,m) satisfies the dispersion relation

$$\omega^2 = N^2(k^2 + l^2)/(k^2 + l^2 + m^2) \qquad (5)$$

The three components of the group velocity vector can be computed by taking partial derivatives of (5) according to

$$C_{gx} = \partial\omega / \partial k \tag{6}$$

$$C_{gy} = \partial\omega / \partial l$$

$$C_{gz} = \partial\omega / \partial m$$

Physically, the group velocity represents the propagation of wave energy through the fluid by the action of oscillating piston-like fluid motions correlated with pressure anomalies. In simple terms, the part of the fluid where the wave is, does work on the part of the fluid where the wave will be, to propagate the wave energy.

From these expressions (6), three important characteristics of internal gravity waves can be seen:

- These waves are dispersive and anisotropic. The wave speed depends on the wavenumber vector, in particular on its orientation relative to the vertical direction.

- The frequency of the gravity wave is always less than the buoyancy frequency N. Disturbances with higher frequency do not propagate.

- The group velocity vector is perpendicular to the wavenumber vector.

These results can be applied to the problem of stationary mountain waves by adding a mean flow (U) to the formulation. A positive mean flow advects the waves to the right, adding a "Doppler" frequency component Uk. We consider waves that propagate to the left relative to the fluid. For simplicity, we reduce the problem to two dimensions (x,z) by setting $l=0$, so that (5) becomes.

$$\omega = Uk - Nk/(k^2 + m^2)^{1/2} \tag{7}$$

Using (6,7) the group velocity vector is

$$\vec{C}g = (U + Nm^2/(k^2 + m^2)^{3/2})\vec{i} + (Nkm/(k^2 + m^2)^{3/2})\vec{k} \tag{8}$$

For the wave to be stationary, the rightward advection and leftward phase propagation must cancel so that ω=0. From (7), this condition establishes a relationship between k and m.

$$m = (N^2/U^2 - k^2)^{1/2} \qquad (9)$$

This relation can be substituted into (8) to determine the group velocity vector in fixed earth-relative coordinates

$$Cg_z = U\hat{k}(1 - \hat{k}^2)^{1/2} \qquad (10)$$

where $\hat{k} = kU/N$ and

$$Cg_x = U\hat{k}^2 \qquad (11)$$

The slope of the ray path is the ratio of the two group velocity components

$$Slope = z/x = Cg_z/Cg_x = \hat{k}^{-1}(1 - \hat{k}^2)^{1/2} \qquad (12)$$

as illustrated in Figure 1 (Bretherton, 1966; Bretherton and Garrett, 1968; Lighthill, 1978).
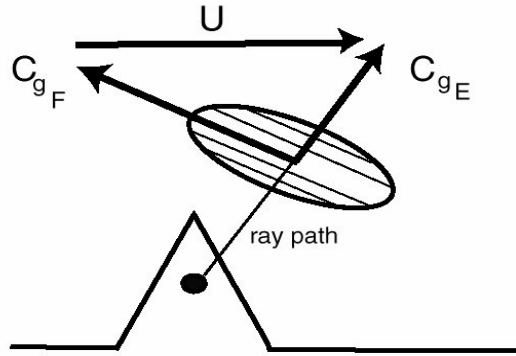
Figure 1: Schematic illustration of the group velocity vector associated with steady two-dimensional mountain waves. The "fluid relative" group velocity C_{gF} is directed upwards and upstream. The "earth relative" group velocity C_{gE}, including advection by the mean flow U, is directed upwards and downstream.

In the hydrostatic limit, k is small compared to N/U and the slope (12) increases towards infinity. Thus, long waves are found directly above the

terrain that generated them. The essential lesson from (12) is that all steady gravity waves will be found either downstream or directly overhead from their source. The nature of the gravity wave dispersion relation (5) is that steady waves will never be found upstream. The term "lee wave" is consistent with this fact; i.e. waves are found on the leeward side rather than the windward side of their generating hills.

3. LINEAR THEORY OF MOUNTAIN WAVES

The equations of linear mountain wave theory, with the Boussinesq approximation, are:

$$Uu_x + Vu_y + U_z w = -(1/\rho_0)p_x \qquad \text{x-momentum} \qquad (13a)$$

$$Uv_x + Vv_y + V_z w = -(1/\rho_0)p_y \qquad \text{y-momentum} \qquad (13b)$$

$$Uw_x + Vw_y = -(1/\rho_0)p_z - (g/\rho_0)\rho' \qquad \text{z-momentum} \qquad (13c)$$

$$u_x + v_y + w_z = 0 \qquad \text{continuity} \qquad (13d)$$

$$U\rho'_x + V\rho'_y + (d\rho/dz)w = 0 \qquad \text{density conservation} \qquad (13e)$$

where x and y are the horizontal coordinates and z defines the vertical coordinate; parallel to the gravity vector. The functions u(x,y,z), v(x,y,z), w(x,y,z), p(x,y,z) and ρ'(x,y,z) are the perturbation velocity component, pressure and density fields. U(z), V(z), ρ(z) are the background environmental wind and density profiles. Subscripts indicate partial derivatives. The derivation of (13) will not be given here, but is found in the references. In (13), the non-linear advection of momentum and density are neglected under the assumption that the disturbance amplitude is small.. The time derivative terms are dropped under the assumption of steady state flow. The steady state assumption is an essential part of mountain wave theory, justified by the steadiness of the incoming flow and the fixed geometry of the terrain.

All the coefficients in (13) are independent of x and y, suggesting that a Fourier transform method might provide a compact solution. As seen below, the Fourier method has the additional advantage of identifying the up- and down-going wave solutions. This identification is necessary for applying the upper boundary condition.

Combining (13) into a single equation for w (x, y, z), and performing a Fourier Transform from physical space (x, y) to Fourier space (k, l) according to

$$\hat{w}(k,l,z) = (1/4\pi^2)\iint w(x,y,z)\exp(-ikx - ily)dx, dy \qquad (14)$$

we obtain a single equation for the transformed vertical velocity; $\hat{w}(k,l,z)$

$$\sigma^2 \hat{w}_{zz} + [(k^2 + l^2)(N^2 - \sigma^2) - \sigma\sigma_{zz}]\hat{w} = 0 \qquad (15)$$

where σ is the intrinsic frequency

$$\sigma = \vec{U} \cdot \vec{\kappa} = Uk + Vl \qquad (16)$$

The intrinsic frequency is the frequency felt by a parcel of fluid moving through the stationary wave field. In stationary waves, it plays the role of the temporal frequency ω seen in (2,5). This transformed equation (15) governs mountain waves in three dimensions. It was first analyzed by Scorer (1956), Wurtele (1957), Crapper (1962) and Sawyer (1962).

In two-dimensional flow, we set l=0 and (15,16) become Scorer's equation.

$$\hat{w}_{zz} + [N^2/U^2 - U_{zz}/U - k^2]\hat{w} = 0 \qquad (17)$$

It is often convenient to use vertical displacement *(η(x, y, z))* as the dependent variable, defined by

$$w(x,y,z) = U\eta_x + V\eta_y \qquad (18)$$

In Fourier space, (18) is

$$\hat{w}(k,l,z) = i\sigma \cdot \hat{\eta}(k,l,z) \qquad (19)$$

The governing differential equation for η(*k, l, z*) combines (15, 16, 19)

$$(\sigma^2 \hat{\eta}_z)_z + (k^2 + l^2)(N^2 - \sigma^2)\hat{\eta} = 0 \qquad (20)$$

Equations (15) and (20) differ slightly, due to the somewhat different effect of vertical shear on vertical velocity and displacement. Note the similar formulation in Chapter 1.

The properties of the solution of (20) depend on the sign of the bracket in the last term (N^2-σ^2). When this coefficient is positive, the solutions are approximately trigonometric in form indicating vertical propagation. When negative, the solutions are approximately exponential. This behavior is

consistent with the idea from Section 2 that when the frequency, in this case the intrinsic frequency, is greater than the buoyancy frequency, the wave can no longer propagate.

An interesting limiting case in mountain wave dynamics is the hydrostatic limit. When the vertical acceleration in equation (13c) is neglected, the transformed equation (20) becomes

$$(\sigma^2 \hat{\eta}_z)_z + (k^2 + l^2)N^2 \hat{\eta} = 0 \qquad (21)$$

The coefficient of the last term is now positive definite, so vertical propagation is guaranteed.

Another interesting situation is when the properties of the atmosphere (i.e. U(z), V(z), N(z)) vary slowly in the vertical. In this case we can write the solution to (17) as

$$\hat{w}(z) = \hat{a}(z)\exp(i\phi(z)) \qquad (22)$$

according to Bretherton (1966). When U(z) and N(z) are constant, a(z) is constant and $\phi(z)$ increases linearly. With slowly varying U and N, the "fast" terms in (17) are

$$(\phi_z)^2 = [N^2/U^2 - U_{zz}/U - k^2] \qquad (23)$$

so that the phase function (ϕ) is given by

$$\phi(z) = \int_0^z [N^2/U^2 - U_{zz}/U - k^2]^{1/2} dz' \qquad (24)$$

For practical purposes, the term U_{zz}/U can usually be neglected in this situation.

The "slow" terms in (17) give, neglecting the small $\hat{a}_{zz}$ term,

$$2\hat{a}_z \phi_z + \hat{a}\phi_{zz} = 0 \qquad (25)$$

so that

$$\hat{a}^2 \phi_z = const. \qquad (26)$$

In the physics literature, the quantity in (26) is referred to as an "adiabatic invariant". As the wave propagates into layers of increasing N(z) or

decreasing U(z), ϕ_z will increase (23) and the amplitude of the perturbation vertical velocity will decrease (26). According to (19) however, the amplitude of the vertical displacements will increase as U(z) decreases, as the parcels spend a longer time in the updraft and downdraft regions. In this scenario, upward changes in the wave field and basic state can promote the role of non-linearity (see Section 5).

In the case when the wind speed decreases to zero at a so-called critical level, the intrinsic frequency (σ in 16) approaches zero and equations (15,17,20,21) become singular. Analysis of the singularity by Booker and Bretherton (1967) showed that this could lead to nearly complete wave absorption. In most cases however, non-linear processes will occur near the critical level (Clark and Peltier, 1984, Winters and D'Asaro, 1994, Dörnbrack et al., 1995, Grubišic and Smolarkiewicz, 1997). A closely related discussion can be found in Chapter 8.

When the wind speed increases and N(z) decreases aloft, ϕ_z will decrease until it becomes zero (23). The asymptotic method described by (22-26) then breaks down. Beyond this point, the wave structure is evanescent and wave energy will be reflected downward.

Mathematical methods for solving (15) and (20) in sheared mean flows have been presented by Klemp and Lilly (1975), Wurtele et al. (1987), Smith (1989a), Grubišić and Smolarkiewicz (1997) and several others. For the present purpose, we return to Sawyer's three-layer formulation. In this approach, the atmospheric profile of velocity and static stability is approximated by three layers with constant properties (U, V, N). The interfaces between layers are at specified heights z_1 and z_2. If wind turning is neglected, the three wind speed values, three stability values and two interface heights amount to eight control parameters. This number of parameters is sufficient to illustrate several ways that wave structure depends on the mean flow. Additional parameters enter the problem through the mountain shape specification. Three layer models have also been discussed by other authors such as Marthinsen (1980).

Our three-layer three-dimensional formulation reduces easily to the two-layer two-dimensional formulation of Scorer and to the one-layer two-dimensional formulation of Lyra and Queney. Thus we can trace the full history of linear mountain wave theory with our model. Our formulation does not include wind turning with height. The turning of the wind gives rise to complex distributed critical layers. Work has just begun on this problem (Broad 1995, Shutts and Gadian 2000)

Within each layer (i =1,2,3) of constant wind and stability, σ_z=0 and N and σ are constant so the solution to (20) is

$$\hat{\eta}_i(k,l,z) = A_i \exp(im_i z) + B_i \exp(-im_i z) \qquad (27)$$

where the vertical wavenumber m is given by

$$m^2 = (k^2 + l^2)(N^2 - \sigma^2)/\sigma^2 \qquad (28)$$

In (27), A_i and B_i are the amplitude coefficients for the up and down-going wave respectively, provided that a consistent sign for "m" is given by sgn(σ). The upgoing wave is characterized by an upwind phase tilt, an upward energy transport and a downward flux of horizontal momentum. When the magnitude of the intrinsic frequency is much smaller than the buoyancy frequency (i.e. $|\sigma| \ll N$), the vertical wavenumber is nearly independent of σ, especially for $l=0$. The wave is hydrostatic and nondispersive. When σ is close to N, the wave is dispersive due to non-hydrostatic effects. When the intrinsic frequency is greater than the buoyancy frequency (i.e. $|\sigma| > N$), the vertical wavenumber "m" in (28) is imaginary and the solutions (27) are exponential rather than trigonometric. In this case, non-hydrostatic effects are dominant and we describe the wave as "evanescent".

Across the interfaces between the layers, continuity of mass and pressure require

$$\Delta\hat{\eta} = 0 \qquad (29)$$

and

$$\Delta\sigma^2\hat{\eta}_z = 0 \qquad (30)$$

assuming that there is no jump in density across the interface. These jump conditions can be derived directly from (20) if desired, by integrating across the interface between layers, and assuming that η and η_z are finite there.

The upper boundary condition requires decay in the upper layer if "m_3" is imaginary. If "m_3" is real, a radiation condition is applied in the top layer by setting the coefficient of the down-going wave equal to zero (i.e. $B_3 = 0$). The linearized lower boundary condition is

$$\eta(x, y, 0) = h(x, y) \qquad (31)$$

which, in Fourier space, is written

$$A_1 + B_1 = \hat{h}(k, l) \qquad (32)$$

In the mountain wave examples discussed in this Chapter, we use an ideal Gaussian hill shape given by

$$h(x, y) = h_m \exp(-(x/a)^2 - (y/b)^2) \qquad (33)$$

as used by Smith and Grønås (1993). In (33), "a" and "b" are the minor and major axes of the elliptical mountain planform shape. The Fourier transform (14) of (33) is

$$\hat{h}(k,l) = (h_m ab / 4\pi) \exp(-(((ka)^2 + (lb)^2)/4))\qquad(34)$$

Expression (34) has elliptical isolines. When the topography is axisymmetric (i.e. a=b), these ellipses become circles and $\hat{h}(k,l)$ decays equally fast with k or l. When the topography is elongated (e.g. a<b), the forced spectrum decays faster in l than in k.

To give the model more flexibility, we introduce a reflection coefficient (q) at the lower boundary to represent partial absorption of down-going waves (Smith et al., 2000). Equation (32) is modified to become

$$A_1 = \hat{h}(k,l) - qB_1\qquad(35)$$

Written in this form, the upgoing wave amplitude (A_1) is the sum of the wave generated by the terrain (h) and the reflected, and phase reversed, down-going wave (B_1). Dissipation of the down-going wave by boundary layer turbulence or by critical layer absorption at the lower boundary can be parameterized by setting $0<q<1$. When q<1, conditions (31,32) are no longer precisely satisfied. Parcel displacements at the lower boundary can be considered to be fluctuations at the top of the boundary layer associated with the absorption mechanism. The slight distortion of the mountain surface can be eliminated by an iterative correction. In practice, this correction may not be needed as the reflected waves return to the lower boundary well downstream of the hill.

To display the linear theory fields, the parcel displacements can be quickly computed from

$$\eta(x,y,z) = \iint \hat{\eta}(k,l,z) \exp(ikx + ily) dk dl\qquad(36)$$

at one or several altitudes using an inverse Fast Fourier Transform (FFT). In (36), $\eta(k,l,z)$ is given by (27) with A and B computed from (26,28,29,35), as shown in the Appendix. For the purposes of this Chapter, evaluation of (36) is carried out on a 1024 by 1024 grid with a grid cell size of one kilometer. The hill (33) is centered in the domain (i.e. at 512, 512).

In the FFT technique, solutions are forced to be periodic. Thus waves that reach the downstream boundary will enter the domain on the upstream boundary. Our large domain includes a significant buffer region to allow waves to decay before they reach the downstream boundary. Nevertheless, the parameters chosen for each case must allow some decay mechanism to operate if well-behaved solutions are sought (see Section 4.4). For display,

we select an interior region with upper left corner at (412,412) and the lower right corner at (712,612). This subdomain thus has a size of 300 by 200 kilometers. Within the subdomain, the hill is located at a point (100,100) from the lower left corner.

4. A CATALOG OF LINEAR THEORY SOLUTIONS

A three-layer three-dimensional formulation allows us to reproduce, in a consistent way, most of the aspects of linear lee wave theory discussed by previous authors. To demonstrate lee wave properties, we have carried out twelve wave field computations with different wind and stability profiles and different mountain shapes (Table 1). All solutions are computed for westerly flow (i.e. U>0 and V=0). The hill has a height of 1000m. The wave fields are shown in planview in Figure 2. The physics of each case is described below, with reference to figure 2 and the relevant literature.

Table 1: Linear theory cases

Fig	Wind U(m/s)	Stability N(10³s⁻¹)	Hill shape a/b/Θ	q	z	z₁/z₂	N₁a/U₁ N₁z₁/U₁	Comment
2a	10	10	10/10/		5		10	UP, hydrostatic
2b	10	10	10/50/0		5		10	UP, hydrostatic, ridge
2c	10	10	2/2/		5		2	UP, dispersive
2d	10	10	2/50/0		5		2	UP, dispersive, ridge
2e	10/22/22	12/8/8	2/2/	0.93	2	2/	2.4/2.4	Trapped
2f	10/22/22	12/8/8	2/50/0	0.90	2	2/	2.4/2.4	Trapped, ridge
2g	18/22/22	12/8/8	2/2/	0.90	2	2/	1.3/1.3	Trapped, no transverse
2h	10/22/10	12/8/12	2/50/0	1.00	2	2/5	2.4/2.4	Leakage
2i	10/22/22	12/8/8	2/50/0	0.50	2	2/	2.4/2.4	Partial bottom absorp.
2j	10/22/22	12/8/8	2/50/0	0.00	2	2/	2.4/2.4	Total bottom absorp.
2k	8/22/22	12/8/8	2/50/0	0.93	2	4/	3.0/6	2 modes
2l	10/22/22	12/8/8	2/50/45	0.90	2	4/	2.4/4.8	Skewed ridge, 2 modes

(UP indicates Upward Propagating waves only. If only one value is given, it applies to all three layers. Distances are given in kilometers).

Blank cells in Table 1 indicate that the solution is independent of this value. For example, the interface altitudes (z_1, z_2) have no meaning if the layers have identical properties. The hill rotation (θ) has no meaning if the hill is axisymmetric. The value of q is irrelevant if there are no layer contrasts to reflect waves downward. The value "z" is the height of the displayed wave field.

While we have chosen to use dimensional quantities in our discussion, the non-dimensional parameter Na/U is given in Table 1 for each case. This parameter is a measure of the degree of hydrostatic balance in the flow. When the parameter is as large as 10, the flow is nearly hydrostatic in all respects.

For smaller values, non-hydrostatic effects, such as dispersion, evanescent behavior and wave trapping occur.

The nondimensional parameter N_1z_1/U_1 is also given in Table 1, when relevant. This parameter provides an estimate of the phase shift across layer #1 for $N/U>k>l$. First mode trapped lee waves require a phase shift between $\pi/2$ and π (i.e. between 1.55 and 3.1 radians). Second mode lee waves require a phase shift between $3/2\pi$ and 2π.

4.1. Vertically propagating waves; hydrostatic

To illustrate a hydrostatic field of mountain waves, we choose a mountain width "a" such that the parameter $Na/U >>1$. Due to the rapid decay of the wavenumber spectrum forced by broad smooth hills (33,34), little energy is put into waves with $k>a^{-1}$. The energetic waves then satisfy $k<<N/U$ so that $\sigma << N$, and the wave motion becomes hydrostatic. In this limit, the vertical wavelength depends only on the orientation of the horizontal wavenumber component, independent of its magnitude. Such waves are dispersive in the aximuthal angle only (28). They have less of a tendency to separate into their components as they propagate. The group velocity vector for normal waves ($l=0$) is vertical, while for oblique waves, it is oriented to the side and downstream.

Two examples of hydrostatic flow in a uniform environment are shown in Figures 2a and b. In Figure 2a, the disturbance is forced by an axisymmetric Gaussian hill. The spectrum generated by such a hill is aximuthally isotropic (34). Extending the ray path argument in Section 2 to hydrostatic 3-D flow, Smith (1980) showed that in each horizontal plane, the wave energy is confined to downstream-trailing parabolic regions given by

$$x = (U / Naz)y^2 \qquad\qquad (37)$$

This parabolic wave energy zone is evident in Figure 2a.

The second example of the hydrostatic limit is flow over a ridge. In this case, the forcing is anisotropic. The dominant waves have $k>>l$. Equation (28) becomes

$$m^2 = (N/U)^2 \qquad\qquad (38)$$

The group velocity for all the wave components making up the disturbance is directed vertically (12). Thus wave energy is found only in the region above the hill. At the level sampled ($z=5000m$), the wave has been phase shifted by about 3/4 of a wavelength so the parcels first fall and then rise as they cross the ridge. An x-z cross section through this wave field would be similar to Queney's celebrated diagram for 2-D hydrostatic waves (see also Section 5.1).
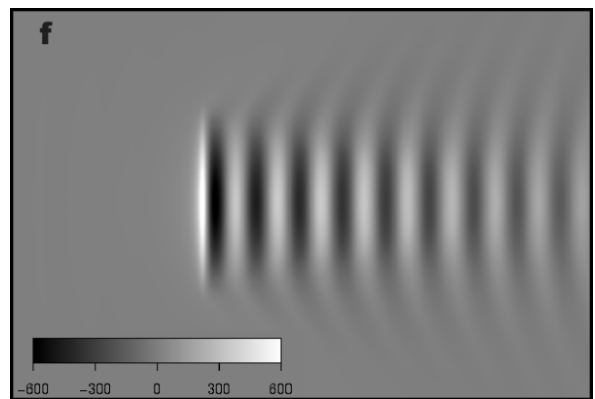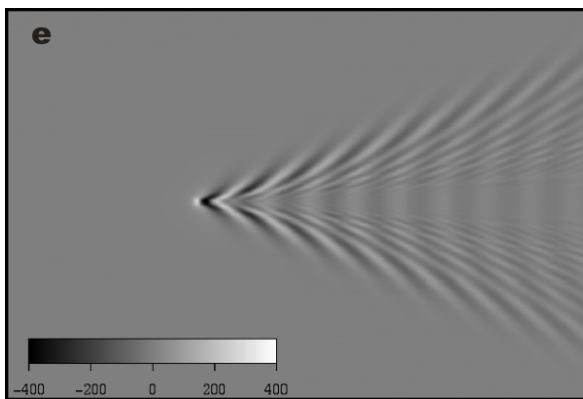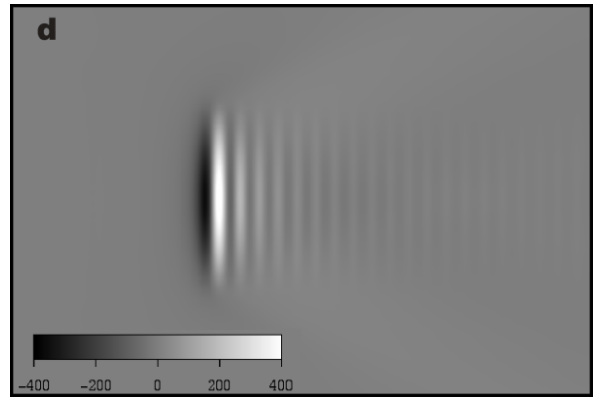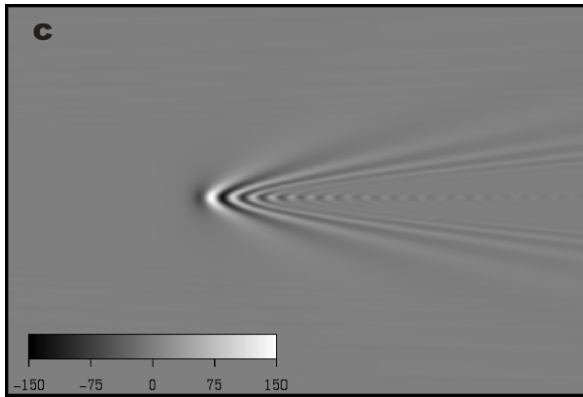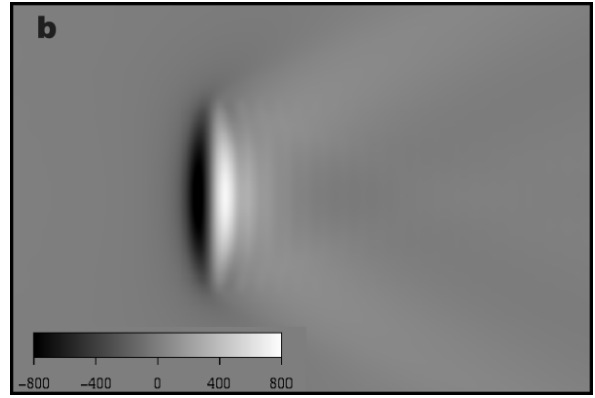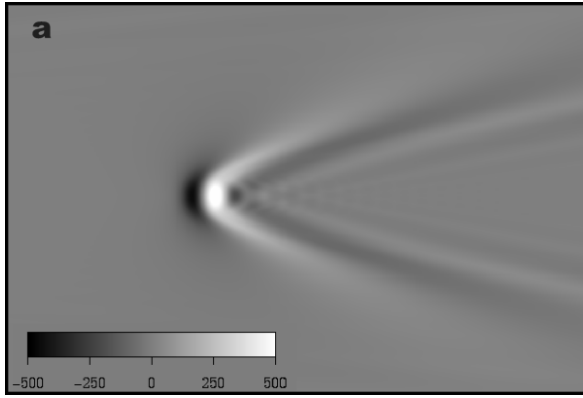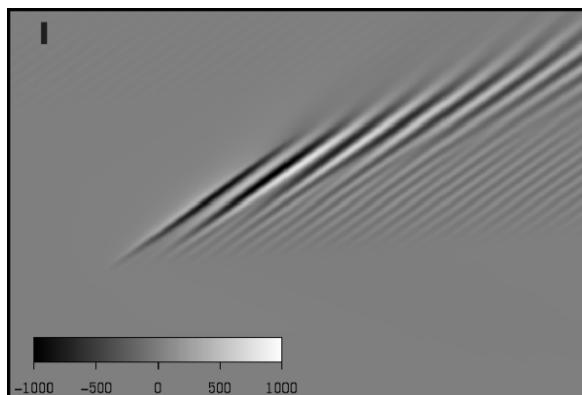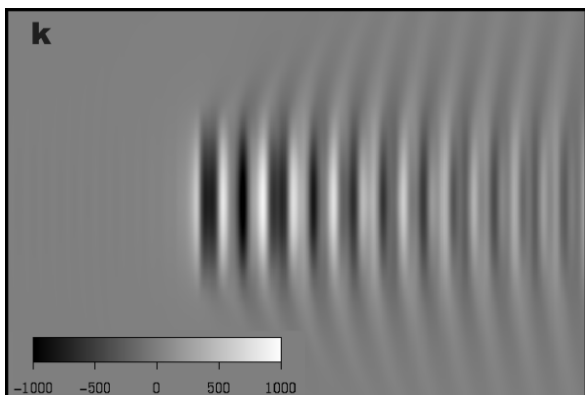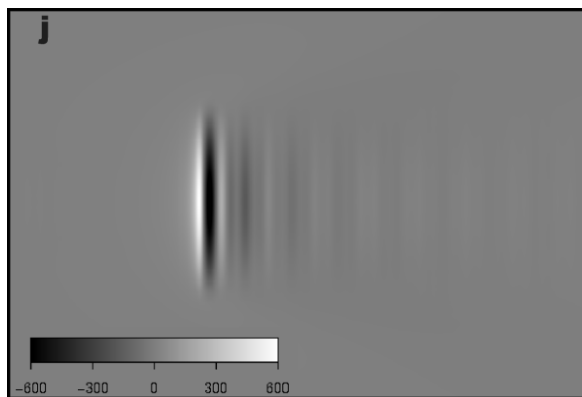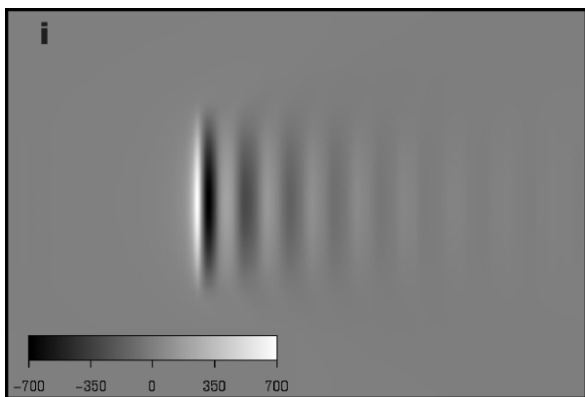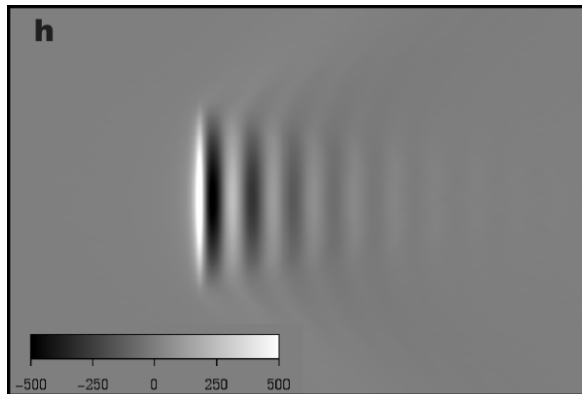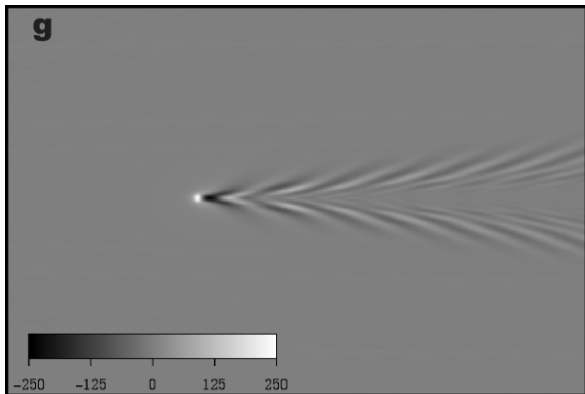
Figure 2: A twelve-part figure with planform views of various linear mountain wave patterns. The vertical displacement of fluid parcels in meters is shown. The conditions for each case are given in Table 1. The fields are computed with a three-layer three-dimensional Fast Fourier Transform model with a 1000m Gaussian hill. The domain shown (300 by 200 km) is part of a larger computational domain (1024 by 1024). The first four diagrams (a-d) show upward propagating waves. The final eight diagrams (e-l) show various trapped or reflected waves.

Other hydrostatic wave patterns are possible. Contrasts between layers allow partial downward reflections not seen in Figures 2a,b. The reflected waves will reflect again from the solid lower boundary (Klemp and Lilly, 1975, Blumen, 1985). A layered representation of the atmospheric profile, such as our three-layer model, may exaggerate these reflections.

The hydrostatic assumption simplifies the derivation of closed form mountain wave solutions such as (37). The drag caused by the pressure difference between the windward and leeward slopes can also be given in closed form. For an axisymmetric Gaussian hill (i.e 33 with a=b) with uniform wind and stability, the drag is

$$D = \frac{1}{2}(\pi/2)^{3/2}\rho_0 NUah_m^2 \tag{39a}$$

For a long ridge (33 with b>>a) the drag per unit length is

$$D_L = \rho_0 NUh_m^2 \tag{39b}$$

where h_m is the local ridge height. If the ridge height varies slowly along its length, (39b) can be integrated along the ridge to obtain the total drag. If the ridge is skewed with respect to the wind direction, U in (39b) should be the wind component perpendicular to the ridge.

4.2. Vertically propagating waves; non-hydrostatic

When the parameter Na/U is near to unity, the wave field will contain both hydrostatic and non-hydrostatic components. The non-hydrostatic components have a group velocity vector with a more downstream orientation. In an elevated horizontal plane therefore, we will see these shorter components downstream of the hydrostatic components. Two examples of this pattern are shown. In both cases we use a uniform wind and stability so that wave components do not change their propagation characteristics as they enter the next layer aloft. Figure 2c shows a 3-D field generated by an axisymmetric Gaussian hill with a=b=2km. Figure 2d shows the wave field from a long ridge. An x-z cross-section through Figure 2d

would be similar to Queney's figure for 2-D dispersing non-hydrostatic waves.

4.3. Trapped lee waves : Diverging and transverse

As shown by Scorer (1949), if the lower layer is slower and/or more stable than the upper layers, waves propagating upward through the lower layer may become evanescent aloft. This will result in the downward reflection of the wave. If the down-coming wave reflects from the earth's solid surface, a resonant cavity will form and a trapped lee wave may exist. The wavelength of the trapped stationary wave will be that which allows the wave's phase propagation upstream to balance the downstream advection, so that the wave is steady. The group velocity is directed downstream when expressed in fixed earth coordinates. As shown by Sawyer (1962), Gjevik and Marthinsson(1978), Marthinsson (1980), Simard and Peltier (1982) and Sharman and Wurtele(1983), trapped lee waves are of two types, diverging and transverse. Diverging waves splay outward from the downstream centerline while the transverse waves are nearly perpendicular to the flow direction.

The resonant condition associated with lee waves can be derived from (27-30) with a homogeneous condition at the lower boundary

$$\hat{\eta}(z = 0) = A_1 + B_1 = 0$$

For a two-layer profile in three dimensions, the result is compactly described by the transcendental condition

$$\text{Cotangent}(m_1 z_1) = -(m_2 / m_1)(\sigma_2 / \sigma_1)^2 \tag{40}$$

where

$$m_1^2 = (k^2 + l^2)(N_1^2 / \sigma_1^2 - 1) > 0 \tag{41}$$

and

$$m_2^2 = (k^2 + l^2)(1 - N_2^2 / \sigma_2^2) > 0 \tag{42}$$

The positive sign conditions in (41) and (42) require that the Scorer Parameter, N/|U|, must decrease aloft. This requirement is called the Scorer Condition. The sets of (k,l) pairs that satisfy (40-42) form families of curves in (k,l) space (Fig 3). These branches lie between the reference lines given by the Scorer Parameter values in the two layers, N_1/U_1 and N_2/U_2. The branch

with the highest wavenumbers is the fundamental mode, with the simplest vertical structure. If a solution branch crosses the *l*=0 axis, there exist transverse lee waves. If no branch crosses the *l*=0 axis, only diverging lee waves exist.

In the original 2-D treatment of lee waves (Scorer, 1949) only transverse waves were considered. In fact, diverging waves may be more common as they encompass a wider parameter range. They require a trapping mechanism, but they do not have to stand steady against the full incoming flow. Their oblique orientation requires them to stand against only a reduced component of the flow speed.

The appearance of a lee wave field depends sensitively on the existence of transverse modes and the forcing of the two lee wave types by the terrain. Here, the forcing ellipse in (k,l) space (34) is a central concern (see Fig 3). If the hill is circular, it will force diverging and transverse waves alike. In the absence of a transverse lee wave mode, diverging waves will still exist. For a ridge oriented across the flow, the forcing is concentrated into waves with small *l*. Diverging waves are not forced. If no transverse mode exists, no lee wave will be found.
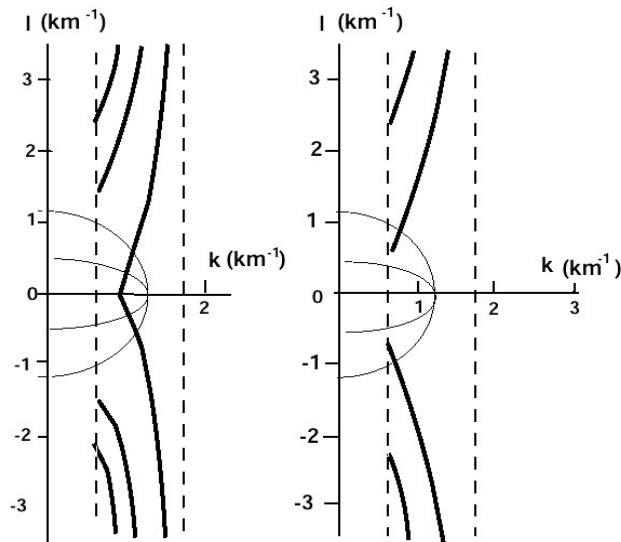
Figure 3. The lee wave singularities (40-42) for a two-layer atmosphere are shown schematically for two cases of westerly flow: a) transverse and diverging waves, b) diverging waves only. Dashed lines indicate the Scorer parameter in the upper and lower layer, delimiting the range of possible lee waves. Two forcing ellipses (34) are also shown; one for an axisymmetric hill and one for a ridge. Only portions of the singular curves that lie inside the forcing ellipse will appear as lee waves. When the forcing ellipse is large and circular, the loss of transverse waves leaves diverging waves. When the ellipse is narrow (i.e. for a ridge) the loss of the transverse wave singularity leaves no significant lee waves. (after Sawyer, 1962).

In Figure 2e, we show a wave field for a simple two-layer atmosphere with a strong enough decrease in Scorer parameter so that both wave types exist. The mountain is circular so both diverging and transverse waves are forced. The diverging waves are easy to identify in the figure. The transverse waves along the centerline are more difficult to see, because of their longer wavelength (i.e. about 25km), but they are substantial. In Fig 2f, we force the same atmosphere with a long ridge. The transverse waves are now strong. They exhibit a slow decay due to dispersion laterally. As the forcing ellipse (34) is narrow, no train of diverging waves is seen. In figure 2g, we return to the small circular hill, but we increase the flow speed so that only diverging waves exist. No waves are seen on the centerline. A Gaussian ridge would generate no lee waves at all with this mean flow.

4.4. Lee wave decay

In the inviscid linear mountain wave problem, there exist three mechanisms of lee wave decay: lateral dispersion, leakage aloft and absorption at the lower boundary. Decay by lateral dispersion was seen in Figures 2e and 2f. No leakage is possible in these cases as the upper layer is infinitely deep and the value of q is taken so large that it only has a decaying influence in the outer domain (not shown).

In Figure 2h, we reduce the depth of layer #2 to 3000m so that lee wave energy can leak through and resume propagating in layer #3. The energy lost in this way results in the downstream decay of wave amplitude. The value of q=1 is chosen in this case so that no absorption occurs at the lower boundary. The wave decays rapidly; only about four crests can be seen before the wave disappears.

In Figure 2i, we return to the deep upper layer but reduce the reflection coefficient at the lower boundary to q=0.5. Every time a downward reflected ray hits the lower boundary, it loses a portion of its energy. The wave amplitude decays rapidly downstream. Only about five wave crests can be seen. The rate of downstream decay depends on the value of q, the depth of the trapping layer and the ray path angle. A shallow layer and steep rays will cause more rapid decay as the waves impinge on the bottom more frequently.

While Figures 2h and 2i look very similar, a detailed analysis of the wave field would reveal significant differences. In the case with leakage aloft, the pressure (p) and vertical velocity (w) are positively correlated in the wave field giving an upward propagation of energy. Likewise, the u and w oscillations are in negative correlation giving a downward flux of horizontal momentum. Mountain drag is carried upward, just as in the vertically propagating examples. With absorption at the lower boundary, both these phase relationships reverse. Energy in the wave train moves downward and the wave drag is returned to the lower boundary from whence it came.

A striking kinematic difference is the tilt of the lee wave structure. Non-decaying trapped lee waves have no vertical tilt of the crest and trough phase lines. Leakage establishes a slight upstream tilt. Low level absorption establishes a downstream tilt.

In Figure 2j, we show a ridge flow with the reflection coefficient q=0. The Scorer Condition is well met, but the downward reflected waves are completely absorbed at the lower boundary. No resonant cavity exists and no trapped lee waves are seen. The wave field includes only dispersing vertically propagating waves (like Figure 2d) and a set of waves reflected downward from the evanescent layer aloft. These two wave trains interfere to give a weak and irregular train. According to Smith et al. (2000), total absorption of the down-going wave will occur when there is a stagnant layer near the surface of the earth.

4.5. Second lee wave mode

To illustrate a second transverse lee wave mode, we deepen the stable layer from 2 to 4 km and decrease the wind speed from 10 to 8 m/s. The non-dimensional number $N_1 z_1 / U_1$ rises to 6. The function $\eta(k,l,z)$ for the second mode has a node in the first layer. Using a long ridge we can compare the pure single mode in Fig 2e with double mode in Fig 2k. The short wave in Figure 2k (i.e. λ=10km) is the fundamental mode. A second mode has a longer wavelength. It beats against the fundamental mode giving an irregular appearance to the lee wave.

As the higher order mode generally has a smaller propagation speed than the fundamental mode, it must compensate by having a longer wavelength. Like the first mode, it must have a sufficient speed to stand steady against the mean flow.

4.6. Left-right asymmetry

Finally, we consider an example without left-right symmetry. We choose a simple two-layer configuration, similar to Fig. 2k, with two transverse modes. The ridge is rotated clockwise by 45 degrees (Figure 2l). For reasons to be explained, we increase the wind speed slightly from 8 to 10 m/s. The new wave field has two wave trains, a longer wavelength train with a ray path angle of about 30 degrees north of east and a shorter wavelength train with a ray angle about 10 degrees north of east.

In the proximity of the ridge, the flow can be considered to be two-dimensional; independent of distance along the ridge. In this local 2-D problem, the incoming flow speed perpendicular to the ridge is reduced by a

factor cosine(45)=0.707 below the actual speed 10m/s. This speed reduction allows a second transverse lee wave mode to exist, as in Figure 2k.

The far wave field in Figure 2l is particularly interesting. Both lee wave families are found in the northeast quadrant of the diagram, indicating that they have a northward component of group velocity. This was anticipated because in the x-y plane the group velocity is normal to the wave crests. Thus the lee wave mode with NE-SW oriented crests has a NW-ward oriented group velocity. The westward component of group velocity is overcome by the mean flow. Its northward component is unopposed by the mean flow and thus the wave train propagates into the NE quadrant. The longer waves have a larger northward component of group velocity than the short waves. The shorter waves barely show their northward component. Because of their different group velocity orientations, the waves separate nicely downstream so that we see each one without interference from the other.

From this example, one can imagine what would happen to a wave field behind a N-S oriented ridge as the wind slowly turned from westerly to southwesterly. Initially of course, the wave field would be located east of the ridge. As the wind turned, the wave field would rotate counterclockwise faster than the wind. When the wind reached SW, the waves would be found, not NE, but NNE of the ridge.

4.7. Applications of Linear Theory

To conclude this Section, we note that linear theory is more than just an idealized model of mountain waves. There are a growing number of observational studies in which linear theory compares well with direct measurements of the atmosphere. Examples include lee waves over western England (Vosper and Mobbs, 1996) and over Mt. Blanc (Smith et al. 2000). The types of patterns shown in Figure 2 are common in satellite images of clouds in the atmosphere. Nevertheless, there is evidence that under certain conditions, non-linearity and dissipation play a role in stratified flow over topography. Examples of nonlinear flow are found over large mountains, e.g downslope winds over the Front Range (Lilly and Zipser, 1972) and waves over the Pyrenees (Bougeault et al., 1997), and over smaller mountains, e.g. lee waves over the Appalachians (Smith, 1976) and the Adriatic Bora (Smith,1987). We review these aspects in the next Section.

5. NONLINEAR AND DISSIPATIVE EFFECTS

The study of nonlinear effects in mountain waves began with R.R. Long's laboratory experiments and his mathematical formulation of a finite amplitude wave equation; the so-called Long's Equation. Long's Equation was elegantly

used by Huppert and Miles (1969) to predict the onset of wave breaking. Long (1955) and Houghton and Isaacson (1968) considered one and two layer hydraulic formulations. Dissipative effects are also important, sometimes forced by non-linearity. In the Section below, we summarize current knowledge of non-linear and dissipative phenomena such as flow splitting, gravity wave breaking, severe downslope winds, hydraulic jumps, rotors and turbulent boundary layers. Some of these subjects have been reviewed in Smith (1989a), Durran (1990), Baines (1995) and Wurtele et al.(1996).

5.1. Flow splitting and gravity wave breaking

One of the most important predictions of mountain wave theory is the onset of flow splitting and gravity wave breaking. Flow splitting is defined as the horizontal splitting of the incoming flow so that it passes around rather than over the mountain peak. Streamline splitting requires that the low-level flow first be decelerated to a stagnation point. Gravity wave breaking, in a uniform background state, begins by the steepening of the wave front and decelerating the flow, leading to overturning. Work on this problem has mostly been confined to the hydrostatic limit where the parameter Na/U is large. In this case, the non-linearity parameter Nh/U plays a dominant role, along with parameters describing the mountain planform shape. We define $H = Nh/U$ as the non-dimensional mountain height. The mountain width plays no role, so intuitive ideas about mountain steepness and splitting must be discarded.

The mechanism of flow deceleration is the same for both flow splitting and wave breaking. In the regions of upward parcel displacement, a positive density anomoly is created by the ascent of denser or potentially cooler air (Figure 4). According to the hydrostatic law, areas of high pressure will exist at the base of these dense fluid anomalies. According to Bernoulli's Law

$$B = p + 1/2\rho_0 U^2 + \rho_0 gz = const \qquad (43)$$

as parcels approach a high pressure region, the speed decreases due to the adverse pressure gradient (Smith and Grubišić, 1993; Vosper and Mobbs, 1997). The height term (ρgz) in (43), once thought to be dominant, plays little role (Smith, 1988, 1990). As the non-dimensional mountain height (H) increases, the strength of the high pressure regions increases at two special locations in the flow; on the windward mountain slope (point B) and at a point directly above the hill at an altitude of approximately $z=(3\pi/2)U/N$ (point A). The relative magnitude of these two deceleration points determines whether flow splitting or gravity wave breaking occurs first (Smith, 1989b; Stein, 1992; Smith and Grønås, 1993; Baines and Smith, 1993; Olafsson and Bougeault, 1996).

For a long ridge, or in strictly two dimensional flow (i.e. x,z), the deceleration at point A is stronger than at point B. Thus wave breaking occurs first, starting approximately when *H*=0.85. For an isolated hill with circular contours, the two points (A and B) are similar in their deceleration potential. Splitting and wave breaking begin approximately when *H*=1.2. In 3-D flow, the lateral dispersion of waves aloft weakens the density anomalies, so a larger hill is required to stagnate the flow.

Once flow splitting begins, the wake region takes on a complex vortical structure which has been investigated in the laboratory (Brighton, 1978, Snyder et al., 1985, Gheusi et al., 2000) and with numerical simulation (Rotunno and Smolarkiewicz, 1991; Miranda and James, 1992). The mechanism of vorticity generation will be discussed in Section 6.

This relatively simple picture for splitting and wave breaking can be modified considerably when the ambient atmospheric profile has vertical structure or a turbulent boundary layer. For example, strong shear or a shallow stable layer aloft may promote wave breaking by a Kelvin-Helmholtz mechanism without requiring deceleration and overturning (See Chapter 8).
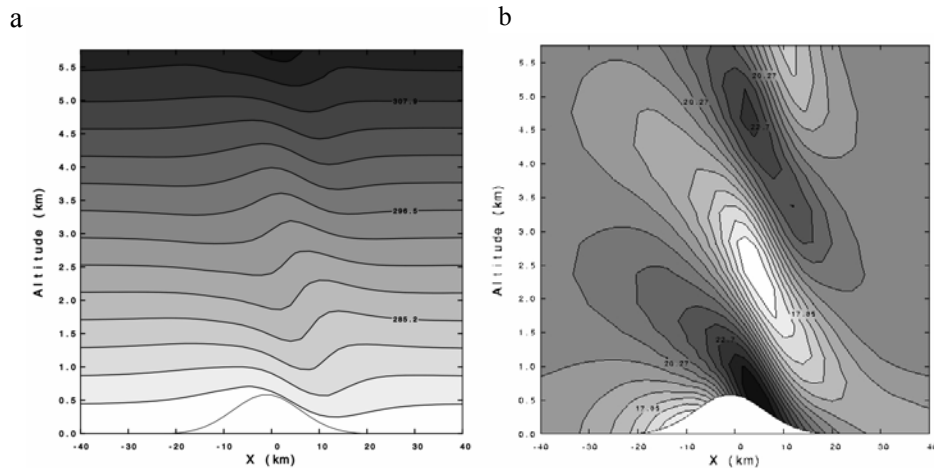
Figure 4. The mountain waves generated by a axisymmetric Gaussian hill, computed with a numerical model. The parameters of the flow are h=600m, a=10km, U=10m/s, N=0.015s^{-1}. The airflow is from left to right. The non-dimensional mountain height is H= 0.9. The left panel (a) shows the vertical displacements of the potential temperature surfaces. The right panel (b) shows the horizontal wind speed. The leftward phase-line tilt shown in Figure 1 is evident in both panels. The displacement field at z=3.3km in panel a resembles that shown in Figure 2.1. Two zones of strong deceleration are seen in panel b. Each zone lies at the base of a region of positive displacement.

5.2. Severe downslope winds

In 1977, Clark and Peltier showed in a numerical simulation that when mountain wave breaking begins in a two-dimensional setting, the entire flow field would transform itself into a new configuration, quite different than the pre-breaking wave field. This new configuration includes spilling or plunging flow down the lee slope, leading to the name "severe downslope wind". This flow also has a magnified mountain drag, turbulence in large region above the lee slope, weaker waves in the stratosphere and some unsteadiness. Peltier and Clark (1985) showed that a similar severe downslope wind structure can be found with smaller mountain heights (i.e. H<0.85) if there is a wind reversal or critical layer at certain altitudes.

A self-consistent theory of downslope winds was put forward by Smith (1985), using Long's Equation for finite amplitude disturbances and an assumption that the low level flow would decouple from any waves which might exist aloft. This model predicts the shape of the isentropes and isotachs, the location of the turbulent flow aloft, the mountain drag, the depth of blocking and the special critical layer heights that can trigger severe winds with small mountains. The theory has been tested in numerical studies (Durran and Klemp,1986,1987; Bacmeister and Pierrehumbert,1988; Crook et al., 1990; Miranda and James, 1992) and limitations have been noted.

5.3. Hydraulic jumps

According to atmospheric observations and numerical simulations, at the downstream limit of the severe downslope wind, the flow speed drops quickly and the streamlines zoom skyward (e.g. Doyle et al., 2000). Such structures have often been equated with the phenomena of the hydraulic jump. This flow structure has been seen both in flows with and without layered profiles upstream. Yet, the hydraulic jump is primarily thought to be layered fluid phenomena. Possibly, when layering is absent upstream, the severe wind descent can create a layered flow where none existed.

The occurrence of a hydraulic jump is related to the fact that a layered flow, with a given flux of mass and momentum, can exist in two so-called conjugate states. Typically, one of these states is subcritical and the other is supercritical (i.e. slower and faster than the long wave speed). When a supercritical flow decelerates, non-linear steepening tendencies act to create a jump, which almost discontinuously converts the fast flow to its slower subcritical conjugate state. An essential property of a jump is that energy is dissipated and the value of the Bernoulli function (43) decreases. This can have consequences for vorticity generation and for the flow pattern further downstream. Baines (1995) gives a thorough treatment of the dynamics of

layered flows, including jump dynamics. The discussion of gravity currents in Chapter 4 is also relevant to this issue.

When the jumps are weak, they can take on a wave-like form, similar to the Morning Glory phenomenon discussed in Chapters 1 and 3. The lee-side hydraulic jump then becomes a mechanism for creating finite amplitude lee waves (Rottman et al, 1996, Nance and Durran, 1998).

Recent work, not included in Baines (1995), is the resolution of the existence and uniqueness problem for jumps in two active fluid layers (Yih and Guha, 1955; Mehotra and Kelly, 1973). New analysis has provided a closed form expression for the Bernoulli loss in each layer resulting from energy dissipation, (Jiang and Smith, 2000). A surprising result was that even when both layers are active in the jump, Bernoulli loss is concentrated in one of the layers. An equal sharing of dissipation seems to be impossible.

5.4. Rotors

The concept of a rotor was put forward in the early papers on mountain waves (i.e. Kuettner, 1939, Queney et al., 1960). According to common usage, the term refers to a compact low level vortex with horizontal axis, downstream of a mountain ridge. The vortex axis lies normal to the mean flow and the sense of rotation is clockwise, if the mean flow is from left to right. The vortex lies underneath, and is causally related to, the first crest of a trapped lee wave. To be defined as a rotor, the vortex must be strong enough to cause reverse flow at the ground. In extreme cases, the reverse flow can be intense and damaging. It can be easily distinguished from a severe downslope flow by its opposite flow direction.

There may be some confusion between a rotor and a hydraulic jump. Both exhibit strong deceleration and upward jumping streamlines. Perhaps rotors may be identified by the reversal of flow near the ground, the reattachment of the flow or the existence of a trapped lee wave.

Numerical models have been shown to capture rotor-like structures, but little theoretical or numerical work has been done to understand the rotor or to more clearly define its character. Derzho and Grimshaw (1997) used Long's Equation to establish a connection between waves and rotors.

5.5. Turbulent Boundary layers

The action of a turbulent boundary layer at the earth's surface has been shown to decrease the amplitude of topographically generated gravity waves (Richard et al, 1989; Olafsson and Bougeault, 1997). Boundary layer waves and turbulence can interact (Carruthers and Hunt, 1990). The separation of the boundary layer by adverse wave-generated pressure gradients may play a

role in rotor formation. A stagnant boundary layer may also absorb waves which have been reflected downward from evanescent layers aloft (Smith et al. 2000). Welch et al. (2000) discusses the blocking and stagnation of boundary layer air in complex terrain.

5.6. The onset of turbulence in breaking gravity waves

The onset of turbulence in breaking gravity waves is a difficult problem involving multiple space and time scales. In spite of frequent aircraft encounters with wave-induced turbulence, the time sequence of turbulence evolution has never been observed. Most numerical models do not resolve smaller scales of motion and so they tell us little about turbulence cascade of energy. Many models simply parameterize the diffusive and dissipative effects of turbulence with an assumed eddy viscosity and diffusivity. These transport coefficients are usually assumed to be strong functions of the resolved Richardson Number or shear magnitude to replicate some properties of shear instability. Other models include a turbulent closure scheme involving a prognostic equation for turbulent kinetic energy (Mellor and Yamada, 1974,1982; Zilitinkevich and Laikhman, 1965, Schumann 1977; Duynkerke, 1988, Trini Castelli and Anfossi, 1997, Xu and Taylor, 1997). These schemes however do not distinguish different scales of turbulence, so they tell us nothing about turbulent cascades. Also, with their current state of development, there is no evidence that their mixing length formulations are appropriate for gravity wave breaking (private communication: Dr. Branko Grisogono). They have been tested only in cases of developed boundary layer turbulence.

The advance of high-speed computers has offered another way forward in this problem. Several authors have recently reported progress using large and/or nested grid arrays that are capable of resolving the first decade of turbulent granulation (Bacmeister, and Schoeberl, 1989, Andreasson et al., 1994, Afanaseyev and Peltier, 1998, Fritts and Isler, 1994, Winters and d'Asaro, 1994; Dörnbrack et al. 1995; Fritts et al. 1996, Schmid and Dörnbrack, 1996, Scinocca 1996, Gheusi et al. 2000). They have been able to identify a sequence of instabilities as the gravity wave steepens. Eventually, the sequence leads to a "three-dimensionalization" of the flow, followed by full cascading turbulence. The resulting turbulent fluxes of heat and momentum can generate macroscopic potential vorticity, as discussed below.

6. THE GENERATION OF POTENTIAL VORTICITY (PV)

The Ertel Potential Vorticity (Ertel, 1942) for compressible flow

$$PV = (1/\rho)\vec{\xi} \bullet \nabla\theta \qquad\qquad (44a)$$

becomes

$$PV = (1/\rho_0)\vec{\xi} \bullet \nabla\rho \qquad\qquad (44b)$$

for Boussinesq flow. Potential vorticity satisfies parcel conservation

$$DPV / Dt = 0 \qquad\qquad (45)$$

in the absence of heat and momentum diffusion. With the Coriolis term neglected, PV provides a useful diagnostic quantity for gravity wave studies and a possible tool to link gravity wave breaking with downstream phenomena such as wakes, eddies, jets and convection (Smith, 1989a,c). Its usefulness arises from the fact that PV remains zero, even in the most non-linear of mountain waves, until wave breaking begins. In laminar waves, the baroclinically generated vorticity vectors lie parallel to density (or isentropic) surfaces and thus the dot product of vorticity and density (or potential temperature) gradient vanishes. Only turbulent transport of heat or momentum or mixing to destroy parcel identity can significantly alter PV in a dry atmosphere (Haynes and McIntyre, 1987, 1990, McIntyre and Norton, 1990). Danielsen's (1990) argument that PV is conserved even in mixing flow is probably incorrect. Once generated, potential vorticity's conservation property (45) allows it to be carried downstream. PV "banners" downstream contain fluid parcels which have passed through the dissipative regions over the mountains. Existing theorems concerning potential vorticity inversion indicate that when balanced flow is reestablished downstream, the PV field can be used to compute the velocity and density anomalies (Blumen, 1972, Hoskins et al., 1985, Raymond, 1993).

The plausibility of PV generation by breaking gravity waves has been established theoretically by detailed investigation of the shallow water system by Schär and Smith (1993a,b), Grubišić et al (1995), Smith and Smith (1995) and Pan and Smith (1999). Samelson (1992), Tjernström and Grisogono (2000) and Jiang and Smith (2000) have examined the shallow water solutions in cases with small or no PV generation. In the shallow water system, the potential vorticity is given by

$$PV = \xi / H \qquad\qquad (46)$$

where ξ is the vertical vorticity and H is the layer depth. In this framework, Bernoulli losses in hydraulic jumps induce lateral gradients in the Bernoulli function (43) which are related to vorticity according to

$$\xi = -(1/U)dB/dn \qquad\qquad (47)$$

in steady flow. In (47), "n" is the direction perpendicular to the streamline. Thus, complex flows with jumps of varying strength will have patterns of potential vorticity downstream. If the generation is weak, these anomalies will advect directly downstream in PV-banners (Figure 5). If the generation is stronger, the PV can wrap itself into stable leeside eddies or alternating drifting vorticies. The merging of two airstreams with differing histories can also generate PV.

A number of field programs have given some support to the potential vorticity generation hypothesis. Smith and Grubišić (1993) showed that large stationary eddies in Hawaii's wake may contain vorticity generated in shallow jumps on the flanks of the island. Smith et al (1997) showed that the stable 300km long wake behind the mountainous island of St. Vincent, can be attributed to wave breaking over the lee slopes (Figure 5). Radar-observed wakes behind the Aleutians have been explained by wave breaking and Bernoulli loss (Pan and Smith, 1998). The recent Mesoscale Alpine Programme, from September to November 1999, verified the predicted PV banners arising from features along the complex crestline of the Alpine massif, particularly in the Rhone Valley and near the Gotthard and Brenner passes (Bougeault, 2000).

Numerical models have shown that they can capture PV generation in continuously stratified flows (Thorpe et al. (1993), Schär and Durran (1995), Smith et al (1995), Aebischer and Schär (1998). The diagnostic evaluation of how PV is generated in numerical models has been more difficult. Schär (1995) provided a theoretical framework. Rotunno et al.(1999) used a numerical model to examine how the conventional viscous terms act to generate PV in dissipating gravity waves.

Examples of the importance of orographic PV generation to downstream weather are appearing in the literature. Hawaii's lee eddy returns volcanic gases to the lee shore, and by weakening the influence of the trade winds there, allows a diurnal sea-land breeze cycle to operate (Smith and Grubišić, 1993). An eddy from the Palmer Divide near Denver controls the spread of urban smog (Crook et al., 1990). Bernoulli loss in breaking waves and PV banners control downstream "gap winds" in the Aleutians (Pan and Smith, 1998). Eddy formation by the mountains of Taiwan is so strong that it can deflect approaching typhoons (Smith and Smith, 1995). South of the Alps, a strong PV eddy can interact with the larger scale baroclinity to trigger cyclogenesis (Aebischer and Schär, 1998). PV generation may also provide a framework for analyzing the influence of wave drag on the general circulation.
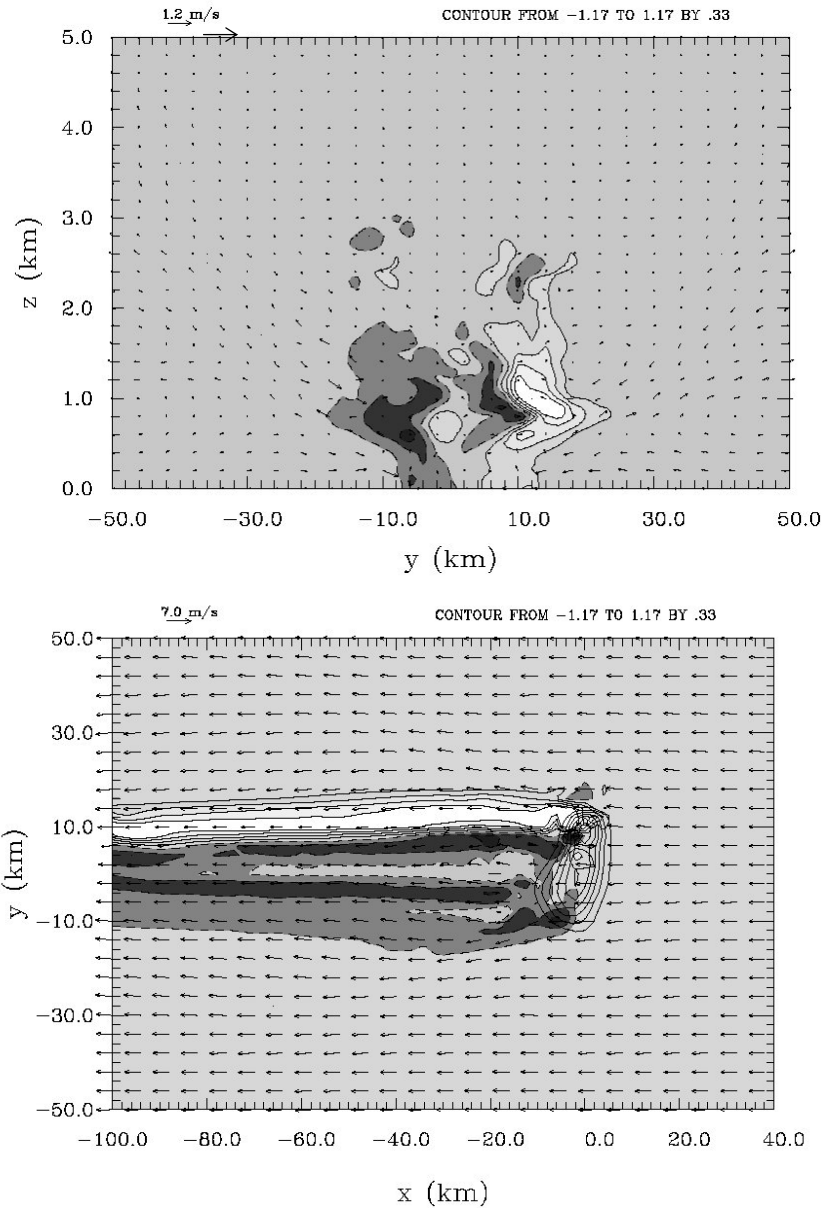
Figure 5: Numerical simulation of PV generated by wave breaking over the mountainous island of St Vincent (from Smith et al., 1997). a) in a y-z cross section 60 km downstream of the island, b) in the x-y plane at an altitude of 1100m. Note that PV=0 upstream of the ridge. PV banners occur as the PV created over the island is advected downstream by the mean flow. The long wake of St Vincent was confirmed by satellite, boat and aircraft surveys.

We conclude this Section by outlining the mechanisms that can generate PV. The question of which mechanism dominates is still unanswered. The analysis of PV generation in a continuously stratified fluid begins with the basic vorticity equations for a Boussinesq fluid. The vector vorticity $\vec{\xi}$ is influenced by advection, stretching and tilting, and is created by baroclinic and viscous terms according to

$$\frac{D\vec{\xi}}{Dt} + \vec{\xi} \cdot \nabla \vec{u} = \frac{1}{\rho_0^2} \nabla \rho \times \nabla P + \frac{1}{\rho_0} \nabla \times \vec{F} \tag{48}$$

where $\vec{F}$ is a viscous force. The potential vorticity (44) is unaffected by stretching, tilting or baroclinic terms and is created and destroyed by viscous and heating terms according to

$$\frac{DPV}{Dt} = \frac{1}{\rho_0} \left(\nabla \times \vec{F} \right) \cdot \nabla \rho + \frac{1}{\rho_0} \vec{\xi} \cdot \nabla \dot{H} \tag{49}$$

where H is the rate of heating per unit mass.

According to Haynes and McIntyre (1987), the generation of PV in a compressible flow can be written in flux form according to

$$\frac{DPV}{Dt} + \nabla \cdot \vec{J}_N = 0 \tag{50}$$

where

$$\vec{J}_N = -\vec{F} \times \nabla \theta - \vec{\xi} \dot{H} \tag{51}$$

is the non-advective flux of P. The first term on the right hand side of (49) or (51) represents viscous torques $\vec{T}$ acting with a component perpendicular to a θ-surface. The second term acts if there is a gradient in the heating rate H along the vorticity vector ($\vec{\xi}$).

Another view of PV dynamics is given by expressing the total flux of PV in steady flow as

$$\vec{J} = \nabla \theta \times \nabla B \tag{52}$$

after Schär (1993). In ideal steady flow, with $\vec{u} \cdot \nabla \theta = \vec{u} \cdot \nabla B = 0$, the $\vec{J}$ vector lies parallel to the flow direction and the PV flux is purely advective (i.e. $\vec{J} = \vec{u} \cdot (PV)$). In the presence of heating ($\dot{H}$) or viscous force ($\vec{F}$),

$\vec{J}$ may have an additional component representing a dissipative non-advective flux. For example, in a wave breaking region, ∇B is directed upstream while $\nabla \theta$ is directed upward. According to (52) the PV flux vector is directed laterally, resulting in a pair of positive and negative PV banners or eddies (Figure 5).

Constraints on the generation of vorticity by viscous stresses (τ_{ij}) can be analyzed using the stress tensor for an isotropic Newtonian fluid.

$$\tau_{ij} = -p\delta_{ij} + 2\mu\left(e_{ij} - \frac{1}{3}\Delta\delta_{ij}\right) \tag{53}$$

where τ_{ij} is the total stress tensor, "p" is the pressure (i.e. usually the thermodynamic pressure), e_{ij} is the rate-of-strain tensor

$$e_{ij} = \frac{1}{2}\left(\frac{\partial u_i}{\partial x_j} + \frac{\partial u_j}{\partial x_i}\right) \tag{54}$$

and $\Delta \equiv e_{kk}$ is the rate of volume change (Batchelor, 1967). The Newtonian model can be formally extended if the viscosity μ (in 53) is allowed to be a function of any rotation-invariant scalar state variable such as the local instantaneous strain rate or Richardson number, or an inherited quantity like turbulent kinetic energy (TKE). This flexibility for μ, encompasses most of the turbulence parameterization schemes proposed in the last 35 years; for example Zilitinkevich and Laikhtman (1965), Lilly (1962), Smagorinsky (1963), Mellor and Yamada (1974, 1982), Schumann (1977), Duynkerke (1988), Dörnbrack (1996), Ying and Canuto (1996), Xu and Taylor (1997), Castelli and Anfassi (1997), Afanaseyev and Peltier (1998).

Using (53,54) and

$$F_i = \frac{\partial \tau_{ij}}{\partial x_j} \tag{55}$$

the torque in (49) is

$$\vec{T} \equiv \nabla \times \vec{F} = \mu\nabla^2\vec{\xi} + \nabla\mu \cdot \nabla\vec{\xi} + \vec{L} \tag{56}$$

In (56), the first two terms diffuse vorticity. The third term can create vorticity when none was present before. We write it schematically as

$$\vec{L} = \vec{L}(\partial u_i / \partial x_i, \partial^2\mu / \partial x_i \partial x_j) \tag{57}$$

indicating that each term in $\bar{L}$ is a product of a first spatial derivative of velocity and a second spatial derivative of viscosity. For convenience, we introduce the term "internal boundary" (I_B) to represent all subregions in the domain where $\dfrac{\partial^2 \mu}{\partial x_i \partial x_j} \neq 0$. An internal boundary is a gradient zone between regions with different viscosity or different turbulent eddy viscosity. Within I_B, it is possible for vorticity to be created by viscous stresses where there was none before. If $\bar{L}$ is oriented with a component perpendicular to a θ-surface, its action will generate potential vorticity.

To illuminate the generation of PV by mountains, we consider the simplest prototype problem; uniform wind and stability approaching a hill in the absence of background rotation. In this case, $\vec{\xi} = 0$ and $PV = 0$ for each incoming fluid parcel. Using (56,57), four distinct PV generation pathways can be identified. Pathway #1 involves the direct creation of vorticity with a cross isentrope component. This can only occur by the action of $\bar{L}$ in (56), within internal boundary regions I_B. Pathway #2 and #3 are two-step processes. First, vorticity is created by the baroclinic mechanism (in 48) as part of the gravity wave propagation mechanism, so $\vec{\xi} \neq 0$ while PV = 0. Then, through the action of heating (Pathway #2; $\vec{\xi} \cdot \nabla H$) or vorticity diffusion (Pathway #3; $\nabla^2 \vec{\xi} \cdot \nabla \theta$) the vorticity is "converted" to potential vorticity. The last possibility, Pathway #4, is that vorticity diffuses in from the lower boundary of the domain.

Rotunno, et al. (1999) have investigated some of these Pathways numerically by using various sets of assumptions about the form of dissipation. To remove P4, they used a free-slip lower boundary and argued, from scale analysis, that curvature effects at the boundary (Batchelor, 1967) are insignificant. P1 and P3 can be eliminated by setting viscosity equal zero, but allowing the diffusion of heat. This assumption isolates P2; the thermal reorientation of the θ-surfaces, so that $\vec{\xi} \cdot \nabla H \neq 0$.

In another simulation, constant non-zero values of viscosity and thermal diffusivity were used, allowing Pathways P2 and P3. In both simulations, conditions were set to give steady flow with weak wave breaking. They concluded that PV generation in 3-D mountain waves occurs primarily by Pathways 2 and 3; i.e. the "conversion" of baroclinic vorticity to potential vorticity. It remains to be learned whether Pathway #1 needs to be considered in fully turbulent wave breaking. P4 will be important in real flows near a no-slip lower boundary.

ACKNOWLEDGEMENTS

APPENDIX 1

The up and down-going wave amplitude coefficients of the 3-layer model, $A_i(k,l)$ and $B_i(k,l)$, are computed from the transform of the terrain $h(k,l)$ and the parameters that define each layer (m_i, σ_i, z_i). The expressions are:

$$A_3 = \hat{h}/(FAE + q \cdot FBE)$$
$$A_1 = FAE \cdot A_3$$
$$B_1 = FBE \cdot A_3$$
$$A_2 = FCE \cdot A_3$$
$$B_2 = FDE \cdot A_3$$

where

$$FCE = (1/2)[1 + R_{32}]\exp(im_3 z_2 - im_2 z_2)$$
$$FDE = (1/2)[1 - R_{32}]\exp(im_3 z_2 + im_2 z_2)$$
$$FAE = (1/4)[(1 + R_{21})(1 + R_{32})]\exp(i(m_2 - m_1)z_1 + i(m_3 - m_2)z_2)$$
$$+ (1/4)[(1 - R_{21})(1 - R_{32})]\exp(-i(m_2 + m_1)z_1 + i(m_3 + m_2)z_2)$$
$$FBE = (1/4)[(1 - R_{21})(1 + R_{32})]\exp(i(m_2 + m_1)z_1 + i(m_3 - m_2)z_2)$$
$$+ (1/4)[(1 + R_{21})(1 - R_{32})]\exp(-i(m_2 - m_1)z_1 + i(m_3 + m_2)z_2)$$

where

$$R_{32} = m_3 \sigma_3^2 / m_2 \sigma_2^2$$
$$R_{21} = m_2 \sigma_2^2 / m_1 \sigma_1^2$$

All these quantities are complex. Note that when the atmospheric conditions are uniform with height, $R_{21}=R_{32}=1$ and the down-going wave amplitudes $B_1=B_2=0$. (Equations from Smith et al., 2000)

REFERENCES

Aebischer, U. and C. Schär, 1998: Low-level potential vorticity and cyclogenesis to the lee of the Alps. *J. Atmos. Sci.*, **55**, 186-207.

Afanasyev, Y. D. and W. R. Peltier, 1998: The three-dimensionalization of stratified flow over two-dimensional topography. *J. Atmos. Sci.,* **55,** 19-39.

Andreassen, Ø., C. E. Wasberg, D. C. Fritts, and J. R. Isler, 1994: Gravity wave breaking in two and three-dimensions: 1. Model description and comparison of two-dimensional evolutions. *J. Geophys. Res.*, **99**, 8095-8108.

Atkinson, B. W., 1981: *Meso-scale Atmospheric Circulations*. Academic Press, 495pp.

Bacmeister, J. T. and R. T. Pierrehumbert, 1988: On high-drag states in nonlinear stratified flow over an obstacle. *J. Atmos. Sci.*, **45**, 63-80.

Bacmeister, J. T. and M. R. Schoeberl, 1989: Breakdown of vertically propagating two-dimensional gravity waves forced by orography. *J. Atmos. Sci.,* **46**, 2109-2134.

Baines, P. G., 1995: *Topographic Effects in Stratified Flows*. Cambridge University Press, 488pp.

Baines, P. G. and R. B. Smith, 1993: Upstream stagnation points in stratified flow past obstacles. *Dyn. Atmos. Oceans*, **18**, 105-113.

Batchelor, G. K., 1967: *An Introduction to Fluid Dynamics*. Cambridge University Press, 615 pp.

Blumen, W., 1972: Geostrophic adjustment. *Geophys. Space Phys.*, **10**, 485-528.

Blumen, W., 1985: Reflection of hydrostatic gravity-waves in a stratified shear- flow. 1. Theory. *J. Atmos. Sci,* **42**, 2255-2263.

Booker, J. R., and F. P. Bretherton, 1967: Critical layer for internal gravity waves in a shear flow. *J. Fluid Mech*., **27**, 513-539.

Bougeault, P., B. Benech, P. Bessemoulin, B. Carissimo, A. Jansa Clar, J. Pelon, M. Petitdidier, and E. Richard, 1997: PYREX: a summary of findings. *Bull. Amer. Meteor. Soc*., **78**, 637-650.

Bougeault, P. et al., 2001: The Mesoscale Alpine Programme Special Observing Period. *Bull. Amer. Meteor. Soc.*, In press.

Bretherton, F. P., 1966: Propagation of groups of internal waves in a shear flow. *Quart. J. Roy. Meteor. Soc*., **92**, 466-480.

Bretherton, F. P. and C. J. R. Garrett, 1968: Wavetrains in inhomogeneous moving media. *Proc. Roy. Soc. London* A, **302**, 529-554.

Broad, A. S., 1995: Linear theory of momentum fluxes in 3-D flows with turning of the mean wind with height. *Quart. J. R. Meteor. Soc.,* **121**, 1891-1902.

Carruthers, D. J. and J. C. R Hunt, 1990: Fluid mechanics of airflow over hills: turbulence, fluxes and waves in the boundary layer. *Atmospheric Processes over Complex Terrain, Meteor. Monogr.*, W. Blumen, Ed., Amer. Met. Soc, No. 23, 83-107.

Clark, T. L. and W. R. Peltier, 1977: On the evolution and stability of finite amplitude mountain waves. *J. Atmos. Sci,* **34**, 1715-1730.

Clark, T. L. and W. R. Peltier, 1984: Critical level reflection and the resonant growth of non-linear mountain waves. *J. Atmos. Sci.,* **41**, 3122-3134.

Crapper, G. D., 1962: Waves in the lee of a mountain with elliptical contours. *Philos. Trans. Roy. Soc. London, A*, **254**, 601-623.

Crook, A. N., T. L. Clark and M. W. Moncrieff, 1990: The Denver cyclone, Part I: Generation in low Froude number flow. *J. Atmos. Sci.*, **47**, 2725-2741.

Danielsen, E. F., 1990: In defense of Ertel's potential vorticity and in general applicability as a meteorological tracer. *J. Atmos. Sci.*, **47**, 2013-2020.

Derzho, O. G. and R. Grimshaw, 1997: Solitary waves with a vortex core in a shallow layer of stratified fluid. *Phys.Fluids*, **9**, 3378-3385.

Dörnbrack, A., T. Gerz, and U. Schumann, 1995: Turbulent breaking of overturning gravity waves below a critical level. *Appl. Sci. Res.*, **54**, 163-176.

Doyle, J. D., D. R. Durran, C. Chen, B. A. Colle, M. Georgelin, V. Grubišić, W. R.. Hsu, C. Y. Huang, D.Landau, Y. L. Lin, G.S. Poulos, W.Y. Sun, D. B. Weber, M. G. Wurtele, and M. Xue, 2000: An intercomparison of model-predicted wave breaking for the 11 January 1972 Boulder windstorm. *Mon. Wea. Rev.*, **128**, 901-914.

Durran, D. R., 1986a: Mountain waves. *Mesoscale Meteorology and Forecasting.* P.Ray, Ed., Amer. Meteor. Soc., 472-492.

Durran, D. R., 1986b: Another look at downslope windstorms. Part I: The development of analogs to supercritical flow in an infinitely deep, continuously stratified fluid. *J. Atmos. Sci.*, **43**, 2527-2543.

Durran, D. R., 1990: Mountain waves and downslope flows. *Atmospheric processes over Complex Terrain*, *Meteor. Monographs*, W. Blumen, Ed., Amer. Met. Soc, No. 23, 59-81.

Durran, D. R., 1998: *Numerical Methods for Wave Equations in Geophysical Fluid Dynamics.* Springer, 472pp.

Durran, D. R. and J. B. Klemp, 1987: Another look at downslope winds, Part II: Non-linear amplification beneath wave-overturning layers. *J. Atmos. Sci.*, **44**, 3402-3412.

Duynkerke, P. G., 1988: Application of the E-e turbulence closure model to the neutral and stable atmospheric boundary layer. *J. Atmos. Sci.*, **45**, 865-880.

Eliassen, A. and E. Palm, 1954: Energy flux for combined gravitational-sound waves. Institute for Weather and Climate Research, Oslo, Publ. No. 1.

Ertel, H., 1942: Ein newer hydrodynamischer Wirbelsatz. *Meteorol. Z.*, **59**, 271-281.

Fritts, D. C., J. F. Garten, and O. Andreassen, 1996: Wave breaking and transition to turbulence in stratified shear flows. *J. Atmos. Sci.*, **53**, 1057-1085.

Fritts, D. C. and J. R. Isler, 1994: Gravity-wave breaking in 2 and 3 dimensions. *J. Geophys. Res.,* **99**, 8109-8123.

Gheusi, F., J. Stein, and O. S. Eiff, 2000: A numerical study of three-dimensional orographic gravity-wave breaking observed in a hydraulic tank. *J. Fluid Mech.,* **410**, 67-99.

Gill, E. A., 1982: *Atmosphere-Ocean Dynamics*. Academic Press, 662 pp.

Gjevik, B. and T. Marthinsen, 1978: Three-dimensional lee-wave pattern. *Quart. J. Roy. Meteor. Soc*., **104**, 947-957.

Gossard, E. E. and W. H Hooke, 1975: *Waves in the Atmosphere*, Elsevier, 456pp.

Grubišić, V., R. B. Smith and C. Schär, 1995: The effect of bottom friction on shallow-water flow past an isolated obstacle. *J. Atmos. Sci*., **52**, 1985-2005.

Grubišić, V. and P. K. Smolarkiewicz, 1997: The effect of critical levels on 3D orographic flows: linear regime. *J. Atmos. Sci.*, **54,** 1943-1960.

Haynes, P. H. and M. E. McIntyre, 1987: On the evolution of vorticity and potential vorticity in the presence of diabatic heating and frictional and other forces. *J. Atmos. Sci.*, **44**, 828-841.

Haynes, P. H. and M. E. McIntyre, 1990: On the conservation and impermeability theorems for potential vorticity. *J. Atmos. Sci.*, **47**, 2021-2031.

Hoskins, B. J., M. E. McIntyre, and A. W. Robertson, 1985: On the use and significance of isentropic potential vorticity maps. *Quart. J. Roy. Meteor. Soc.*, **111**, 877-946.

Houghton, D. D. and E. Isaacson, 1968: Mountain winds. *Studies in Num. Anal.*, **2**, 21-52.

Huppert, H. E., and J. W. Miles, 1969: Lee waves in stratified flow, Part 3: Semi-elliptical obstacle. *J. Fluid Mech.*, **35**, 481-496.

Jiang, Q. and R. B. Smith, 1999: V-waves, bow waves and wakes in supercritical hydrostatic flow. *J. Fluid Mech.*, **406**, 27-53.

Jiang, Q. and R. B. Smith, 2000: Idealized hydraulic jumps in two-layer flow, Part II: Under a passive layer. *Tellus*, **52A**, In Press.

Klemp, J. B. and D. K. Lilly, 1975: The dynamics of wave-induced downslope winds. *J. Atmos. Sci.*, **32**, 320-339.

Kuettner, J., 1939: Moazagotl und Fohnwelle, *Beitr. Phys. frei Atmos.*, **25**, 79-114.

Lighthill, J., 1978: *Waves in Fluids*, Cambridge University Press, 504p.

Lilly, D. K. and E. J. Zipser, 1972: The Front Range windstorm of 11 January 1972 - a meteorological narrative. *Weatherwise,* **25**, 56-63.

Long, R. R., 1953: Some aspects of the flow of stratified fluids, A theoretical investigation. *Tellus*, **5**, 42- 58.

Long, R.R., 1955: Some aspects of the flow of stratified fluids, III. Continuous density gradients. *Tellus,* **7**, 341-357.

Lyra, G., 1943: Theorie der stationären Leewellenströmung in freier Atmosphäre. *Z. Angew. Math. Mech.*, **23**, 1-28.

Marthinsen, T., 1980: Three-dimensional lee waves, *Quart. J. Roy. Meteor. Soc.*, **106**, 569-580.

McIntyre, M. E. and W. A. Norton, 1990: Dissipative wave-mean interactions and the transport of vorticity and potential vorticity. *J. Fluid Mech.*, **212**, 403-435.

Mehrotra, S. C., and R. E. Kelly, 1973: On the question of non-uniqueness of internal hydraulic jumps and drops in a two-fluid system. *Tellus*, **25**, 560-567.

Mellor, G. L. and T. Yamada, 1974: A hierarchy of turbulence closure models for planetary boundary layers. *J. Atmos. Sci.*, **31**, 1791-1806.

Mellor, G. L. and T. Yamada, 1982: Development of a turbulence closure model for geophysical fluid problems. *Rev. Geophys Space Phys.*, **20**, 851-875.

Miranda, P. M. and I. N. James, 1992: Non-linear three-dimensional effects on gravity wave drag: Splitting flow and breaking waves. *Quart. J. Roy. Meteor. Soc.,* **118**, 1057-1081.

Nance, L. B. and D. R. Durran, 1998: A modeling study of nonstationary trapped mountain lee waves. Part II: Nonlinearity. *J. Atmos. Sci.,* **55**, 1429-1445.

Olafsson, H. and P. Bougeault, 1996: Nonlinear flow past an elliptic mountain ridge. *J. Atmos. Sci,* **53**, 2465-2489.

Olafsson, H. and P. Bougeault, 1997: The effect of rotation and surface friction on orographic drag. *J. Atmos. Sci*, **54,** 193-210.

Pan, F. and R. B. Smith, 1998: Gap winds and wakes: SAR observations and numerical simulations. *J. Atmos. Sci.*, **56**, 905-923.

Peltier, W. R. and T. L. Clark, 1979: Evolution and Stability of Finite-Amplitude Mountain Waves .2. Surface-Wave Drag and Severe Downslope Windstorms. *J. Atmos. Sci,* **36**, 1498-1529.

Queney, P., 1947: Theory of perturbations in stratified currents with applications to airflow over mountain barriers. Dept. of Meteorology, Univ. of Chicago, Misc. Report No. 23.

Queney, P., G. Corby, N. Gerbier, H. Koschnieder, and H. Zierep, 1960: The airflow over mountains. WMO Tech. Note No. 34, World Meteorological Organization, Geneva, 135pp.

Raymond, D. J., 1993: Nonlinear balance and potential-vorticity thinking at large Rossby number. *Quart. J. Roy. Meteor. Soc.*, **118**, 987-1015.

Richard, E., P. Mascart, and E. C. Nickerson, 1989: Role of surface friction in downslope windstorms. *J. Appl. Meteor.*, **28**, 241-251.

Rottman, J. W., D. Broutman, and R. Grimshaw, 1996: Numerical simulations of uniformly stratified fluid flow over topography. *J. Fluid Mech.*, **306**, 1-30.

Rotunno, R., V. Grubišić, and P. K. Smolarkiewicz, 1999: Vorticity and potential vorticity in mountain wakes. *J. Atmos. Sci.*, **56**, 2796-2810.

Rotunno, R. and P. K. Smolarkiewicz, 1991: Further results on lee vorticies in low-Froude-number flow. *J. Atmos. Sci.*, **48**, 2204-2211.

Samelson, R. M., 1992: Supercritical marine-layer flow along a smoothly varying coastline. *J. Atmos. Sci.*, **49**, 1571-1584.

Sawyer, J. S. 1962: Gravity waves in the atmosphere as a three-dimensional problem. *Quart. J. Roy. Meteor. Soc.*, **88**, 412-427.

Schär, C., 1993: A generalization of Bernoulli's Theorem. *J. Atmos. Sci.*, **50**, 1437-1443.

Schär, C and D. R. Durran, 1997: Vortex formation and vortex shedding in continuously stratified flows past isolated topography. *J. Atmos. Sci.*, **54**, 534-554.

Schär, C. and R. B. Smith, 1993a: Shallow-water flow past isolated topography. Part I: Vorticity production and wake formation. *J. Atmos. Sci.*, **50**, 1373-1400.

Schär, C. and R. B. Smith, 1993b: Shallow-water flow past isolated topography. Part II: Transition to vortex shedding. *J. Atmos. Sci.*, **50**, 1401-1412.

Schmid, H., and A. Dörnbrack, 1996: Simulation of breaking gravity waves during the south foehn of January 7-13, 1996: *Beitr. Phys. Atmos.*, **72**, 287-301.

Schumann, U., 1977: Realizability of reynolds stress turbulence models. *Phys. Fluids*, **20**, 721-725.

Scinocca, J. F., 1995: The mixing of mass and momentum by Kelvin-Helmholtz billows. *J. Atmos. Sci.*, **52**, 2509-2530.

Scorer, R. S. 1949: Theory of waves in the lee of mountains. *Quart. J. Roy. Meteor. Soc.*, **82**, 75-81.

Scorer, R. S. and M. Wilkinson, 1956: Waves in the lee of an isolated hill. *Quart. J. Roy. Meteor. Soc.*, **82**, 419-427.

Sharman R. D. and M. G. Wurtele 1983: Ship waves and lee waves. *J. Atmos. Sci*, **40**, 396-427.

Shutts, G. J. and A. Gadian, 2000: Numerical simulations of orographic gravity waves in flows which back with height. *Quart. J. Roy. Meteor. Soc.*, **125**, 2743-2765.

Simard, A. and W. R. Peltier, 1982: Ship waves in the lee of isolated topography. *J. Atmos. Sci,* **39**, 587-609.

Smith, R. B., 1976: Generation of lee waves by the Blue Ridge. *J. Atmos. Sci.*, **33**, 507-519.

Smith, R. B. 1979, Influence of mountains on the atmosphere: *Adv. Geophys.*, **21**, 87-217.

Smith, R. B., 1980: Linear theory of stratified hydrostatic flow past an isolated mountain. *Tellus,* **32**, 348-364.

Smith, R. B., 1985: On severe downslope winds. *J. Atmos. Sci,* **42**, 2597-2603.

Smith, R. B., 1987: Aerial observations of the Yugoslavian Bora. *J. Atmos. Sci.*, **44**, 269-297.

Smith, R. B., 1988: Linear-theory of stratified flow past an isolated mountain in isosteric coordinates. *J. Atmos. Sci,* **45** , 3889-3896.

Smith, R. B., 1989a: Hydrostatic Airflow Over Mountains. *Adv. Geophys.,* **31**, 1-41.

Smith, R. B., 1989b: Mountain-induced stagnation points in hydrostatic flow. *Tellus*, **41A**, 270-274.

Smith, R. B., 1989c: Comment on "Low Froude number flow past three dimensional obstacles. Part I: Baroclinically generated lee vorticies". *J. Atmos. Sci.*, **46**, 3611-3613.

Smith, R.B., 1990: Why can't stably stratified air rise over high ground? *Atmospheric processes over Complex Terrain. Meteor. Monographs*, W. Blumen, Ed., Amer. Meteor. Soc., No. 23, 105-107.

Smith, R. B., A. C. Gleason, P. A. Gluhosky and V. Grubišić, 1997: The wake of St. Vincent*. J. Atmos. Sci.*, **54**, 606-623.

Smith, R. B. and S. Grønås, 1993: The 3-D mountain airflow bifurcation and the onset of flow splitting. *Tellus*, **45A**, 28-43.

Smith, R. B. and V. Grubišić, 1993: Aerial observations of Hawaii's wake. *J. Atmos. Sci.*, **50**, 3728-3750.

Smith, R. B., S. Skubis, J. Doyle, A. Broad, C. Kiemle, and H. Volkert, 2000: Gravity waves over Mt. Blanc. Submitted to *Quart. J. Roy. Meteor. Soc.*

Smith, R. B. and D. F. Smith, 1995: Pseudoinviscid wake formation by mountains in shallow-water flow with a drifting vortex. *J. Atmos. Sci.*, **52**, 436-454.

Snyder, W. H., R. S. Thompson, R. E. Eskridge, R. E. Larson, I. P Castro, J. I. Lee, J. C. R Hunt, and Y Ogawa, 1985: The structure of strongly stratified flow over hills: dividing streamline concept. *J. Fluid Mech.*, **152**, 249-288.

Stein, J., 1992: Investigation of the regime diagram of hydrostatic flow over a mountain with a primitive equation model, Part I: Two-dimensional flows. *Mon. Wea. Rev*., **120**, 2962-2976.

Thorpe, A. J., H. Volkert and D. Heimann, 1993: Potential vorticity of flow along the Alps. *J. Atmos. Sci.,* **50***, 1573-1590.*

Tjernström, M. and B. Grisogono, 2000: Simulations of supercritical flow around points and capes in a coastal atmosphere. *J. Atmos. Sci*., **57**, 108-135.

Trini Castelli, S. and D. Anfossi, 1997: Intercomparison of 3D turbulence parameterisations for dispersion models in complex terrain derived from a circulation model. *Il Nuovo Cimento*, **20C**, 287-313.

Turner, J. S., 1973: *Buoyancy Effects in Fluids*. Cambridge University Press, 367pp.

Vosper, S. B. and S. D. Mobbs, 1996: Lee waves over the English Lake District. *Quart. J. Roy. Meteor. Soc.*, **122**, 1283-1305.

Vosper, S. B. and S. D. Mobbs, 1997: Measurement of the pressure field on a mountain. *Quart. J. Royal Meteor. Soc*., **123**(537 Part A): 129-144.

Welch, W., P. Smolarkiewicz, R. Rotunno, and B. Boville, 2000: The large scale effects of flow over periodic mesoscale topography. Submitted to *J. Atmos. Sci.*

Winters, K. B. and E. A. D'Asaro, 1994: Three-dimensional wave instability near a critical level. *J. Fluid Mech.*, **272**, 255-284.

Wurtele, M. G., 1957: The three-dimensional lee wave. *Beitr. Phys. Atmos.,* **29**, 242-252.

Wurtele, M. G., R. D.Sharman and A. Datta, 1996: Atmospheric Lee Waves, *Annual Rev. Fluid Mech*., **28**, 429-476.

Wurtele, M. G., R. D. Sharman and T. L. Keller, 1987: Analysis and simulations of a troposphere-stratosphere gravity wave model. Part 1. *J. Atmos. Sci.,* **44**, 3269-3281.

Xu, D. and P. A. Taylor, 1997: On turbulence closure constants for amtospheric boundary-layer modelling: Neutral stratification. *Bound.- Layer Meteor.*, **84**, 267-287.

Yih, C. S. and C. R. Guha, 1955: Hydraulic jump in a fluid system of two layers. *Tellus*, **7**, 358-366.

Zilitinkevich, S. S. and D. L. Laikhtman, 1965: On closure of a system of equations for turbulent flow in the atmospheric boundary layer – Tr. GGO, **167**, 44-48.